

## Search for forced oscillations in binaries

### III. Improved elements and the detection of line-profile variability of the B4V + A6V: system AR Cassiopeiae

D.E. Holmgren<sup>1,\*</sup>, P. Hadrava<sup>1</sup>, P. Harmanec<sup>1</sup>, P. Eenens<sup>2</sup>, L.J. Corral<sup>3</sup>, S. Yang<sup>4,\*</sup>, H. Ak<sup>5</sup>, and H. Božić<sup>6</sup>

<sup>1</sup> Astronomický ústav, Akademie věd České Republiky, CZ-251 65 Ondřejov, Czech Republic  
(holmgren@brandonu.ca; had(hec)@sunstel.asu.cas.cz)

<sup>2</sup> Departamento de Astronomia, Universidad de Guanajuato, Apartado 144, 36000 Guanajuato, GTO, Mexico (eenens@carina.astro.ugto.mx)

<sup>3</sup> Instituto de Astrofísica de Canarias, c/Vía Lactea s/n, E-38200 La Laguna, Spain (lcorral@iac.es)

<sup>4</sup> Department of Physics and Astronomy, University of Victoria, P.O. Box 3055, Victoria, B.C., V8W 3P6, Canada (yang@beluga.phys.uvic.ca)

<sup>5</sup> Ankara University, Science Faculty, Astronomy and Space Science Department, Tandoğan, 06100 Ankara, Turkey  
(ak@astrol.science.ankara.edu.tr)

<sup>6</sup> Hvar Observatory, Faculty of Geodesy, Zagreb University, Kačićeva 26, 10000 Zagreb, Croatia (hbozic@geodet.geof.hr)

Received 11 June 1998 / Accepted 9 March 1999

**Abstract.** An analysis of a new and extensive set of spectroscopic observations of the early-type binary system AR Cas, based also on spectral disentangling, has led to the discovery of the spectrum of the secondary star and of line-profile variations of the B4V primary star. A revised spectroscopic orbit based on these and published data is presented. We also present new photometric data, which have allowed us to improve the solution of the light curve and demonstrate the presence of apsidal motion. Determination of the basic physical parameters of the binary has allowed us to conclude that the system combines the main-sequence primary with an A6V: secondary, possibly an Am star. The consistency of our model of AR Cas is documented by a comparison of model atmosphere flux profiles with the profiles recovered from the spectral disentangling. Analysis of the He I 667.8 nm line indicates that line profile variability is present, and that these variations may be periodic.

**Key words:** stars: binaries: spectroscopic – stars: fundamental parameters – stars: individual: AR Cas

#### 1. Introduction

This is the third in a series of papers devoted to the investigation of line profile variability in early-type binary systems, and to determining new physical parameters for these systems. The motivation for this project (known as “SEFONO”) has been discussed in detail in the two previous papers on V436 Per (Harmanec et al. 1997) and  $\beta$  Sco A (Holmgren et al. 1997).

*Send offprint requests to:* D. Holmgren, Department of Physics and Astronomy, Brandon University, Brandon, Manitoba, R7A 6A9, Canada

\* Guest investigator, Dominion Astrophysical Observatory, Victoria, BC, Canada

In the present paper, we discuss new observations, physical parameters, and detection of line profile variability in the eclipsing system AR Cas (HD 221253, HR 8926). A preliminary account of this work was presented by Holmgren (1996). AR Cas has been the subject of a number of spectroscopic and photometric studies in the past (see Sects. 3 and 4), but these have been limited by the rather awkward orbital period of  $\sim 6.0663$  days, which is well-determined from the photometry. AR Cas has also gained some notoriety from the fact that the secondary star has never been detected spectroscopically. To the best of our knowledge, the present study is the first one based on an analysis of digital spectra. An important result of the present work has been the detection of the secondary spectrum through the use of spectral disentangling. Moreover, spectra obtained from observatories in both Europe and North America have allowed us to circumvent the problem of the orbital period and, therefore, to sample the radial-velocity (RV hereafter) curve properly. From these data, we have obtained reliable physical parameters for both components of AR Cas. Also, we have used the Hipparcos parallax for this star to obtain a mass ratio independent of the orbital analyses and to confirm our detection of the secondary. Finally, the digital spectra have allowed us to detect line-profile variability in the early-type primary star.

#### 2. Observations and reductions

##### 2.1. Spectroscopy

New spectroscopic observations were obtained at Ondřejov, Victoria (DAO), and San Pedro Mártir. The main features of the spectrograph and detector configurations used for these new observations are summarized in Table 1. For further details on the DAO 21181 and 9681 spectrographs, we refer the reader to Richardson (1968). We now describe some specific details of the new observations.

**Table 1.** New spectroscopic data sets

Observer	Epoch	Instrument	Spectrograph	Detector	Dispersion	Wavelength Range
	(HJD-2400000)				(nm mm <sup>-1</sup> )	(nm)
SY	50273–50421	DAO 1.8m	21181	UBC 4096 CCD	1.0	616.5–671.8
SY	50273–50421	DAO 1.2m	9681	UBC 4096 CCD	1.0	616.5–671.8
SY	50823–50825	DAO 1.2m	9681	SITe-2 1850 CCD	0.48	649.3–675.0
DH	50290–50294	DAO 1.8m	21181	SITe-2 1850 CCD	1.0	650.6–668.6
DH	50295–50296	DAO 1.2m	9681	SITe-2 1850 CCD	0.48	660.5–672.7
PE	50335–50341	SPM 2.0m		CCD	0.4–1.6	369.6–760.0
Ondřejov	50239–50515	2.0m		1872 Reticon	1.7	630.0–670.0

**Table 2.** RV data sets

Dataset	Epoch	No. of RVs	Weight	Source
	HJD-2400000			
1	18131–18622	19	0.15	A
2	27666–28056	26	1.9	B
3	30648–30653	10	5.2	C
4	40082–40476	44	5.1	D
5	40441–40889	29	1.7	E
6	43770–43829	64	1.3	E
7	50239–50515	6	7.6	F
8	50273–50421	18	3.8	G
9	50290–50825	23	3.5	H
10	50335–50341	6	0.6	I

Abbreviations of column “Source”:

A Baker (1910); B Luyten et al. (1939); C Petrie (1944); D Gorza & Heard (1971); E Gaida & Seggewiss (1981); F Ondřejov Reticon 1872 spectra; G DAO UBC CCD 4096; H DAO SITe-2 CCD; I San Pedro Mártir CCD

The Ondřejov Reticon data were obtained at a dispersion of 1.7 nm mm<sup>-1</sup>, centred approximately on H $\alpha$ . The exposure times for these spectra vary from 0.5 hr to 2.5 hr, with a corresponding signal-to-noise ratio in the range  $200 \leq S/N \leq 450$ . Flat-field, bias, and calibration arc exposures were obtained before and after each stellar spectrum. Reductions of these data were done using the SPEFO program, written by Dr. J. Horn (Horn et al. 1996, Škoda 1996).

The datasets denoted by SY were obtained by S. Yang, and were reduced by him using IRAF in the usual fashion. The exposure times for these data were typically 10 minutes, with a signal-to-noise of  $\sim 300$ . Extensive series of flat-field lamp and bias frames were obtained at the start and end of each night, with arc spectra being interleaved between the stellar exposures. SPEFO was used for the purposes of wavelength calibration and continuum rectification of 1-D frames.

Two sets of data were obtained by D. Holmgren (DH) at the DAO during July and August of 1996. For the first set, the 1.8 m telescope and Cassegrain spectrograph operating at a dispersion of 1.0 nm mm<sup>-1</sup> was used. For the second data set, the 1.2 m telescope and coudé spectrograph operating at 0.48 nm mm<sup>-1</sup> were used. A slit width of 250  $\mu$  was used for both sets of observations. In both cases, calibration arc frames were obtained

before and after each stellar frame. During each night, series of 10 flat-field lamp and 10 bias exposures were obtained at the beginning, middle, and end of the night. These were later averaged for the processing of the stellar data frames. For the 1.8 m data, exposure times for the stellar data were typically 10 minutes, with  $S/N \sim 300$ , while for the 1.2 m data exposure times of 40 minutes were used, giving  $S/N \sim 400$ . The data obtained by DH were reduced using the MIDAS package, from initial extraction and flat-fielding through to wavelength calibration. Continuum rectification of these data was done using SPEFO.

The high-resolution spectra of 1996 September 8–15 were obtained by P. Eenens (PE) and L. Corral at the 2-meter telescope at San Pedro Mártir (Mexico) with the echelle spectrograph and a 2000  $\times$  2000 CCD. The echelle grating has 79 lines mm<sup>-1</sup> and its blaze angle is 63° 43', giving dispersions ranging from 0.4 to 1.6 nm mm<sup>-1</sup>. The chosen slit width of 150  $\mu$ m corresponded to 2 arcseconds on the sky. Almost every observation was made of three consecutive exposures of 120 seconds, to increase the signal in the blue part of the spectrum without saturating the long wavelength orders. For wavelength calibration, spectra of a Thorium–Argon lamp and a Helium–Argon lamp were taken immediately before and after each observation. The data were reduced by P. Eenens and L. Corral using the MIDAS package.

Additionally, we also compiled RVs from the astronomical literature. The journal of all available RV data is in Table 2.

## 2.2. Photometry

Several light curves of AR Cas were published. The star has also been observed by Hipparcos and three of us obtained new *uvby* and *UBV* observations in the period from November 1997 to October 1998 at Turkish National Observatory (TNO), Hvar, and San Pedro Mártir. Basic information on all available data sets can be found in Table 3.

Very fortunately, all observers used the same comparison star 1 Cas = HD 218376 which has colours very similar to those of AR Cas. We, therefore, derived V, B, and U magnitudes of AR Cas adding the *UBV* magnitudes of 1 Cas to the published magnitude differences AR Cas– 1 Cas. For 1 Cas, we adopted:

$$V = 4^m.836, \quad B = 4^m.799, \quad U = 3^m.939.$$

**Table 3.** Journal of the photoelectric observations of AR Cas

Dataset No.	Epoch HJD-2400000	No. of obs.	No. of nights	Passbands used
1	21482.8–22699.6	225	70	yellow
2	unknown	173	?	<i>V</i>
2	unknown	171	?	<i>B</i>
2	unknown	168	?	<i>U</i>
3	40062.5–40455.6	238	31	<i>V</i>
3	40062.5–40455.6	256	33	<i>B</i>
4A	32480.7–32495.8	77	3	<i>B</i>
4B	36806.6–36894.8	97	9	<i>UVBGRI</i>
5	47866.6–49042.0	129	34	<i>H<sub>p</sub></i>
6	50760.3–50763.6	29	2	<i>wvby</i>
7	50854.2–51086.3	40	6	<i>UBV</i>
8	51055.9–51065.9	29	8	<i>UBV</i>

Abbreviations of column “Dataset”:

1 S21 = Stebbins (1921); 2 HC62 = Huffer & Collins (1962): observations secured in 1954 and 1956; 3 CR71 = Catalano & Rodonò (1971); 4A GK73A = Gordon & Kron (1973), Lick 0.30-m; 4B GK73B = Gordon & Kron (1973); Lick 0.50-m; 5 HIP = Perryman et al. (1997); 6 HA97 = this paper, TNO observations; 7 HB98 = this paper, Hvar observations; 8 PH98 = this paper, San Pedro Mártir observations

These standard *UBV* values were derived by us from a careful reduction of Hvar and San Pedro Mártir calibrated all-sky observations. More details on the data reduction and homogenization can be found in Appendix A. The Hipparcos *H<sub>p</sub>* magnitudes were transformed into Johnson *V* using the transformation formula given by Harmanec (1998).

Very regrettably, the observations of Huffer & Collins (1962) were only published in the form orbital phase vs. flux in each passband. The HJDs of these 1954 and 1956 observations are not known and we do not use them in this study. Almost all data sets were transformed into the standard *UBV* system by us, the only exceptions being datasets 3 and 4 which remain in their instrumental systems.

### 3. Light-curve solutions

#### 3.1. Locally derived solutions

Since there has been some controversy about the presence of an observable apsidal motion in the system, we first derived solutions of individual light curves based on a sufficient number of observations, reasonably well covering the eclipses. The solution for the light curve by Gordon & Kron (1973) was unstable due to the poor quality of their data and is not, therefore, included. To restrict the number of free elements, we kept the eccentricity of the orbit at a value of 0.24, well constrained from the spectroscopic solutions (see below). All solutions presented here were obtained using program FOTEL (Hadrava 1990). The errors of the elements were derived from the covariance matrix (in this paper, we will take “errors” to signify standard deviations  $\pm\sigma$  taken from the diagonal elements of the covariance matrix). Stebbins (1921) presents  $\omega = 37^\circ.25$ , whereas here we

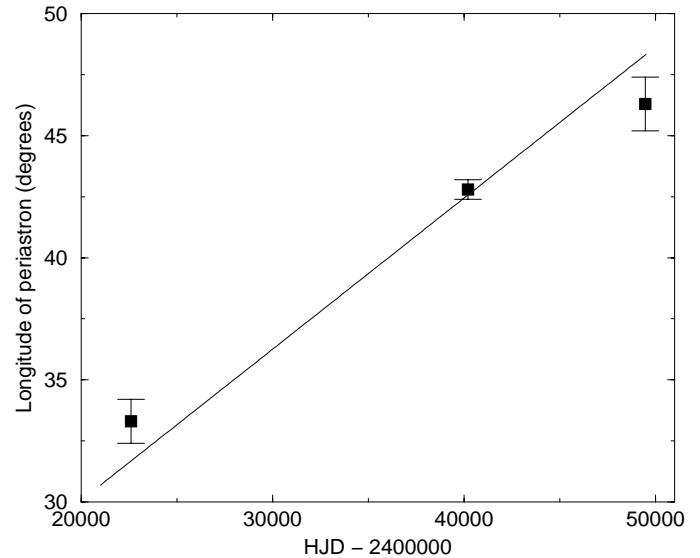


**Fig. 1.** A plot of the values of the longitude of periastron, derived from the individual light curves (squares), vs. time. The line is the apsidal motion  $\omega(t)$  from the combined (final) light curve solution (see text for details)

find  $33^\circ.3 \pm 0^\circ.9$ . The difference in these values is most probably due to the method of light curve solution used. We consider our FOTEL solution to be more realistic than the Russell-type solution computed by Stebbins; differences between the Russell method and more modern techniques based on better physical models are to be expected.

An inspection of Table 4 where the local solutions are presented shows that the apsidal motion is undoubtedly present. This is illustrated in Fig. 1 where we plot the value of the periastron passage for each solution along with its calculated error vs. time. For comparison, we show the computed apsidal motion  $\omega(t)$  based on the rate found from the light curve solution for all of the data (see next section). The epoch for  $\omega(t)$  is the periastron epoch for this combined solution. The *V* light curve based on the transformed Hipparcos and our new data is shown in Fig. 2.

#### 3.2. Final solution of the light curve

Given the finding that the apsidal motion is indeed present, we used all photometric data for which times of observations were available to calculate the final light-curve solution. FOTEL allows one to include the rate of the apsidal motion and also individual magnitudes at light maxima among the elements calculated during the solution. The epochs of primary ( $T_{prim.ecl.}$ ) and secondary eclipse ( $T_{sec.ecl.}$ ) were computed from the periastron epoch  $T_{peri}$ , since the latter was solved for in the least-squares solution. Also, we have used the value of periastron epoch from the spectroscopic solution as a starting value for the periastron epoch in the light curve solution. The final solution is given in Table 5. Note that the values for the combined *V* and *B* at the bottom of this table are mean values computed from the calibrated data only.

**Table 4.** FOTEL light-curve solutions for individual light curves. All epochs are in HJD–2400000 and the local solutions are identified by abbreviations from notes to Table 3. Also,  $e = 0.240$  has been assumed. Here and in other tables, the value of  $\omega$  always refers to the periastron epoch given for each solution

Element	S21	CR71	HIP+HA97+HB98+P H98
$P$ (d)	$6.066321 \pm 0.000037$	$6.06631 \pm 0.00037$	$6.066343 \pm 0.000014$
$T_{peri.}$	$22585.888 \pm 0.011$	$40196.567 \pm 0.006$	$49465.971 \pm 0.014$
$\omega$ (deg.)	$33.3 \pm 0.9$	$42.8 \pm 0.4$	$46.3 \pm 1.1$
$r_1$	$0.1836 \pm 0.0056$	$0.1870 \pm 0.0058$	$0.1967 \pm 0.0050$
$r_2$	$0.0598 \pm 0.0030$	$0.0537 \pm 0.0023$	$0.0649 \pm 0.0032$
$i$ (deg.)	$86.7 \pm 2.5$	$84.1 \pm 0.8$	$82.8 \pm 0.9$
rms (mag.)	0.0119	0.0053	0.0067

**Table 5.** Final FOTEL light-curve solution for all available photometric data with known times of observations. All epochs are in HJD–2400000 and the light levels at the light maximum in individual band-passes and data sets (in magnitudes) are identified by abbreviations from notes to Table 3. Also,  $e = 0.240$  has been assumed

Element	final
$P$ (d)	6.0663170
$P_{anomal.}$ (d)	$6.0663801 \pm 0.0000049$
$T_{peri.}$	$36847.9404 \pm 0.0055$
$T_{prim.ecl.}$	36848.4454
$T_{sec.ecl.}$	36846.1107
$\omega$ (deg.)	$41.82 \pm 0.47$
$d\omega/dt$ (deg. yr $^{-1}$ )	$0.212 \pm 0.025$
$r_1$	$0.1826 \pm 0.0022$
$r_2$	$0.0580 \pm 0.0012$
$i$ (deg.)	$85.34 \pm 0.50$
$L_1(V)$	0.974
$L_1(B)$	0.978
$V_{S21}$ (mag.)	$4.8540 \pm 0.0009$
$V_{CR71}$ (mag.)	$4.8517 \pm 0.0006$
$V_{GK73B}$ (mag.)	$4.8303 \pm 0.0014$
$V_{HIP}$ (mag.)	$4.8871 \pm 0.0006$
$V_{HA97}$ (mag.)	$4.8828 \pm 0.0006$
$V_{HB98}$ (mag.)	$4.8801 \pm 0.0021$
$V_{PH98}$ (mag.)	$4.8807 \pm 0.0015$
$B_{CR71}$ (mag.)	$4.7671 \pm 0.0014$
$B_{GK73A}$ (mag.)	$4.7641 \pm 0.0005$
$B_{GK73B}$ (mag.)	$4.7529 \pm 0.0016$
$B_{HB98}$ (mag.)	$4.7641 \pm 0.0015$
$B_{PH98}$ (mag.)	$4.7617 \pm 0.0015$
$U_{GK73B}$ (mag.)	$4.1300 \pm 0.0018$
$U_{HB98}$ (mag.)	$4.0958 \pm 0.0025$
$U_{PH98}$ (mag.)	$4.1126 \pm 0.0024$
rms (mag.)	0.0101
$\bar{V}_{1+2}$ (mag.)	4.883
$V_1$ (mag.)	4.912
$V_2$ (mag.)	8.814
$(B - V)_{1+2}$ (mag.)	-0.120
$(B - V)_1$ (mag.)	-0.125
$(B - V)_2$ (mag.)	0.099

The solution shows that the secondary star is about  $4^m 0$  fainter than the primary in  $V$  and  $B$ . Regrettably, it was not

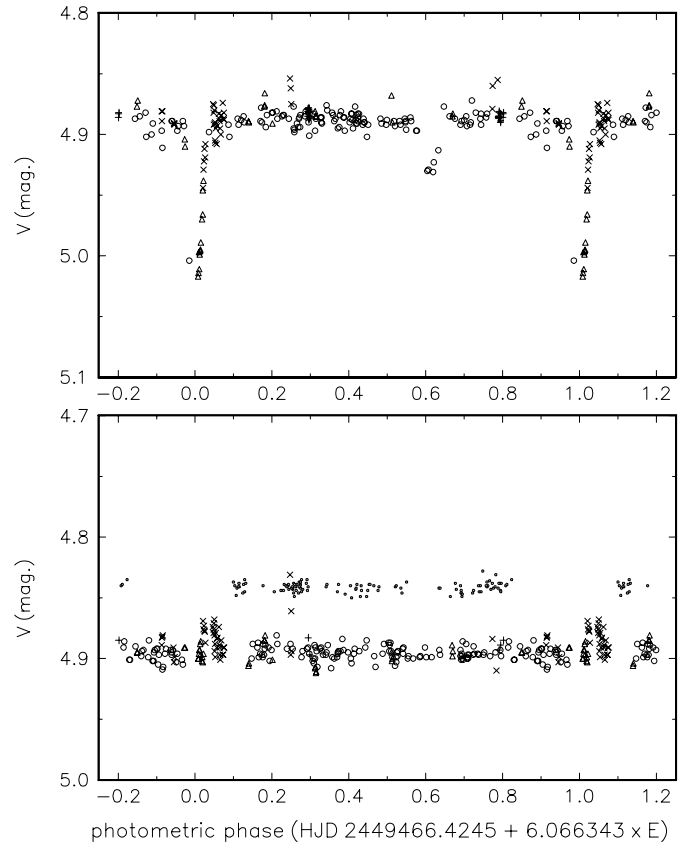


**Fig. 2.** The  $V$  light curve of AR Cas for the Hipparcos and our new data corresponding to the solution of Table 4. The upper panel refers to AR Cas, while the bottom one shows  $\sigma$  Cas – 1 Cas for differential observations, and all-sky 1 Cas observations for the transformed Hipparcos data. The circles represent Hipparcos data, pluses TNO data, crosses Hvar data, and triangles San Pedro Mártir data

possible to derive either the individual  $U$  magnitudes or their ratio since the existing light curves do not cover the phases of the secondary minimum well enough. This – together with larger observational errors in  $U$  – made such a solution impossible at present. We note, however, a very good mutual agreement of individual light levels at maxima for all data sets transformed into the standard  $UBV$  system. For completeness, we mention that we only used the  $y$  passband (which can be directly re-

**Table 6.** AR Cas cross-correlation radial velocities from He I 667.8 nm.

File	HJD−2400000	Phase (peri)	RV (km s <sup>−1</sup> )	<i>O</i> − <i>C</i> (km s <sup>−1</sup> )
10834	50239.5602	0.5174	−35.7	7.7
11023	50252.5269	0.6549	−13.9	−2.7
11130	50279.5700	0.1128	−27.2	−4.6
11667	50360.5315	0.4589	−52.8	0.5
11749	50369.2910	0.9029	51.1	0.0
12685	50515.3069	0.9728	42.0	−0.8
13838	50273.9870	0.1925	−45.7	3.5
17720	50311.7492	0.4174	−47.5	9.6
17750	50311.8043	0.4265	−55.7	0.4
18863	50335.7181	0.3685	−71.2	−9.7
19427	50336.9869	0.5777	−31.0	−1.9
19812	50338.0040	0.7454	20.0	3.3
11870	50354.9082	0.5319	−35.5	3.5
11871	50354.9259	0.5348	−35.6	2.8
12165	50355.9105	0.6971	0.7	−1.6
12256	50355.9789	0.7084	2.1	−3.5
12317	50356.0161	0.7146	5.0	−2.4
12369	50356.0429	0.7190	8.6	−0.2
13391	50381.9231	0.9852	39.6	−0.8
13728	50382.8790	0.1428	−37.7	−4.1
14976	50420.6477	0.3687	−58.7	2.8
15100	50420.7977	0.3935	−59.7	−0.1
15535	50421.5957	0.5250	−41.6	−1.2
15556	50421.6119	0.5277	−40.1	−0.3
9674	50290.8649	0.9747	48.6	2.5
9703	50290.9517	0.9890	39.2	−2.2
9923	50292.9705	0.3218	−61.6	−0.8
9925	50292.9783	0.3231	−62.9	−2.1
9978	50293.8394	0.4651	−45.7	2.8
9980	50293.8470	0.4663	−48.4	−0.1
10021	50293.9824	0.4886	−50.0	−5.3
10023	50293.9908	0.4900	−49.2	−4.8
15386	50687.9068	0.4250	−51.9	2.0
15479	50688.7477	0.5636	−28.4	1.6
20154	50767.8516	0.6034	−18.1	2.6
15022	50684.8608	0.9229	52.6	−2.4
2147	50868.6374	0.2174	−48.6	3.7
2165	50868.6921	0.2265	−51.0	2.9
21204	50783.5941	0.1985	−50.4	−2.0
907	50825.6117	0.1249	−26.6	−2.5
916	50825.6425	0.1300	−29.7	−3.5
945	50825.6810	0.1363	−29.2	−0.4
952	50825.7181	0.1424	−31.0	0.2
983	50825.7591	0.1492	−32.1	1.6
987	50825.7901	0.1543	−31.1	4.4
1003	50825.8305	0.1610	−36.7	1.1
1009	50825.8582	0.1655	−38.6	0.7
2018	50335.8464	0.3897	−73.6	5.2
4036	50337.9248	0.7323	−6.6	−0.4
5035	50338.9194	0.8963	32.7	−0.6
6018	50339.9069	0.0590	1.0	14.0
7024	50340.8798	0.2194	−82.3	−8.3
8024	50341.8882	0.3856	−89.0	−9.8

**Table 7.** AR Cas KOREL radial velocities for H $\alpha$ .

HJD	Phase (peri)	$V_{pri}$ (km s <sup>−1</sup> )	<i>O</i> − <i>C</i> (km s <sup>−1</sup> )	$V_{sec}$ (km s <sup>−1</sup> )	<i>O</i> − <i>C</i> (km s <sup>−1</sup> )
50239.5602	0.5542	−27.32	0.00	86.44	0.00
50252.5269	0.6917	−3.14	−5.65	1.63	9.95
50279.5700	0.1496	−14.37	−1.51	46.64	6.23
50360.5315	0.4957	−36.26	−0.41	113.54	−0.16
50369.2910	0.9396	66.79	−1.20	−223.57	−7.67
50515.3069	0.0096	53.26	−1.05	−173.64	−1.53
50273.9870	0.2293	−33.16	2.17	112.67	0.89
50311.7492	0.4542	−41.93	−1.45	133.61	5.48
50311.8043	0.4633	−40.30	−0.71	127.71	2.39
50335.7181	0.4053	−44.09	0.00	139.68	0.00
50336.9869	0.6145	−18.38	−2.44	24.17	−26.14
50338.0040	0.7821	30.74	1.30	−94.39	−0.64
50381.9231	0.0220	46.77	−2.27	−156.62	−0.93
50382.8790	0.1796	−25.41	−2.35	72.63	−0.60
50420.6477	0.4055	−40.97	2.98	139.24	−0.54
50420.7977	0.4302	−40.98	1.36	132.33	−2.39
50421.5957	0.5618	−25.29	0.60	82.95	0.46
50421.6119	0.5645	−25.43	0.00	81.02	0.00
50354.9082	0.5687	−24.79	0.00	78.53	0.00
50354.9259	0.5716	−24.27	0.00	76.87	0.00
50355.9105	0.7339	12.03	−2.47	−46.96	−0.78
50356.0161	0.7513	16.34	−3.42	−54.06	8.84
50687.9068	0.4618	−40.95	−1.21	127.94	2.14
50688.7477	0.6004	−18.14	0.70	60.29	0.79
50767.8516	0.6402	−11.85	−1.69	16.19	−16.23
50684.8608	0.9596	64.06	−2.87	−209.58	3.27
50868.6374	0.2542	−43.70	−4.47	108.14	−16.76
50868.6921	0.2632	−44.40	−3.98	108.73	−19.92
50783.5941	0.2353	−35.96	0.31	113.84	−1.57
50825.6117	0.1617	−17.17	−0.08	46.83	−7.86
50825.6810	0.1731	−19.22	1.73	66.88	−0.02
50825.7591	0.1860	−24.87	0.00	79.38	0.00
50825.8305	0.1977	−29.54	−1.44	106.75	17.13
50768.7710	0.7918	31.56	−1.10	−115.13	−11.61
50654.0025	0.8728	55.32	−2.23	−184.93	−1.79
50713.9570	0.7560	22.70	1.51	−65.18	2.29
50823.6322	0.8354	47.29	0.52	−149.39	−1.32
50823.7088	0.8480	49.61	−1.07	−160.68	−0.21
50732.9334	0.8842	59.20	−1.27	−193.04	−0.98
50733.0197	0.8984	65.02	1.48	−203.59	−1.79

duced to  $V$ ) from the HA97 data since these observations only cover 2 nights outside eclipses and do not allow determination of Strömgen colours for individual components.

We note that the maximum light level in  $V$  seems to vary slightly and possibly cyclically with time. As discussed in Appendix A, the transformation errors in  $V$  should be smaller than some 0<sup>m</sup>.02. Therefore, the differences up to 0<sup>m</sup>.05 in  $V$  at maximum might be real. The possibility of a secular light variation should be kept in mind and tested by future accurate observations.

#### 4. RV measurements and orbital solutions

All spectra were measured for radial velocities using two techniques: cross-correlation (e.g., Holmgren et al. 1997) and disentangling via the KOREL program (Hadrava, 1997). The latter was used to see if a secondary spectrum could be extracted, and to obtain a set of RVs independent of the ccf measurements. Moreover, KOREL allows a separation of the telluric lines which are present in many of the stellar lines studied here.

##### 4.1. Cross-correlation RVs

The cross-correlation function (ccf hereafter) measurements were initially limited to the He I 667.8 nm line since this line shows obvious LPV, and because the Si II 634.0–637.0 nm lines have a telluric contribution. A spectrum of the slowly rotating B2V star  $\zeta$  Cas (B2IV, HR 153, HD 21566,  $v \sin i = 18 \text{ km s}^{-1}$ ) was used as a template for the cross-correlation measurements. A radial velocity of  $1.8 \text{ km s}^{-1}$  was adopted for this star on the basis of line-by-line measurements. The wavelength limits for these ccf measurements were 666.5–669.0 nm. Radial velocities of the primary star of AR Cas were measured by fitting a parabola to each ccf peak. These measurements are summarized in Table 6. Note that these data are arranged first according to dataset and then by Julian date; the first column of Table 6 is the file number for each spectrum. Telluric line corrections were employed to bring the Ondřejov and DAO RVs onto effectively the same instrumental system (see Horn et al. 1996 for details). Note that the phases in Table 6 have been computed with respect to the time of periastron passage, using the anomalistic period  $P_a = 6.0663801 \text{ d}$ .

An attempt was made to detect the secondary component of AR Cas directly by cross-correlation of the weak metal lines in the region 633.0–641.0 nm (Ne I 633.4 nm, Si II 634.7 nm, Si II 637.1 nm, N II 637.4 nm, Ne I 638.3 nm, Ne I 640.2 nm). For these measurements, the whole segment of spectrum between 633.0 nm and 641.0 nm was used. However, the telluric lines are strong enough in relation to the weak secondary spectrum to effectively mask it out. The only plausible alternative is to decompose these lines using KOREL.

##### 4.2. Disentangling, orbital solution and detection of the secondary

Disentangling orbital solutions using the KOREL program were computed for a number of different spectral lines: Si II 634.7 nm, Si II 637.1–Ne I 638.3 nm, Ne I 640.2 nm,  $H\alpha$ , and He I 667.8 nm. The orbital period from our final light-curve solution was kept fixed in all these solutions. Note that apsidal motion has *not* been included in the KOREL solutions since the new data cover only a very small part of the apsidal period (hence the difference in phases between Tables 6 and 7). Not all spectra were used in the solution due to internal limitations of KOREL, and also because a few spectra were of relatively poor quality when compared to the others. Moreover, in some datasets many spectra were taken at the same or similar phases for the purpose of detecting LPV,

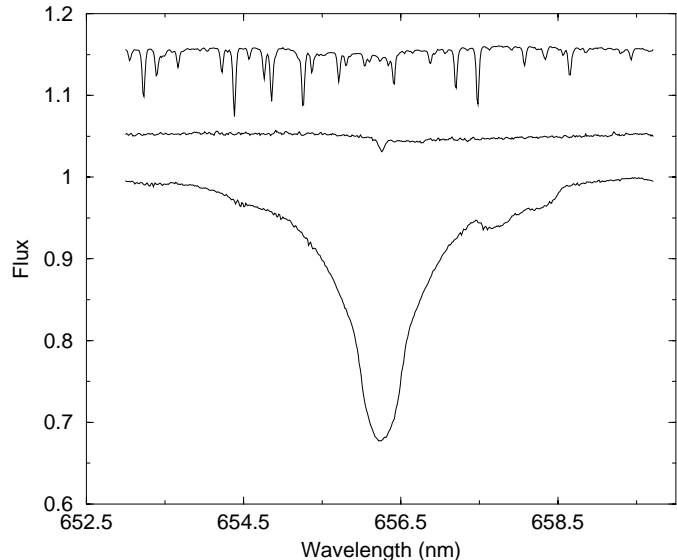


**Fig. 3.** The normalized  $H\alpha$  line profile for AR Cas reconstructed by KOREL. Profiles of the secondary (middle) and telluric lines (top) have been shifted upward for clarity

so to use all of the spectra available at a given phase would have resulted in some points being given an unjustifiably large weight.

A weak secondary spectrum was recovered for all lines except for He I 667.8 nm and Ne I 640.2 nm. The corresponding velocity curves for the secondary have varying degrees of scatter, but KOREL did produce plausible secondary line profiles. The spectrum is most likely that of an A-type star, but further discussion of this topic is deferred to Sect. 5. The KOREL solution for He I 667.8 nm had the added benefit of allowing the line profile variability to be investigated (cf. Sect. 6). For the  $H\alpha$  line, binary parameters were converged simultaneously with the telluric parameters, also allowing for the variable intensities of the latter. The resulting decomposed line profiles for the  $H\alpha$  and He I 667.8 nm lines of the primary and secondary are shown in Figs. 3 and 4. A similar approach was used for the two Si II lines, as these show a telluric component. We have also decomposed but not computed a solution for the Mg II 448.1 nm line, as the latter is present on the echelle spectra (there are too few echelle spectra to permit an independent solution). This line reveals very clear evidence of a secondary spectrum, and we will return to it later (see Sect. 5.2). The radial velocities determined by KOREL are too extensive to be tabulated here in full, but the results for  $H\alpha$  are presented in Table 7 as they are probably the best, and also representative of the results for the other lines. The final KOREL solutions are summarised in Table 8 (in which  $\sigma_1$  denotes the rms scatter about the fit for each line). The spectroscopic orbital elements determined from the cross-correlation measurements were used as a guide in choosing the starting solution for KOREL. We have presented errors for all KOREL solutions based on inverting the covariance matrix at the solution point. However, the differences between parameters for *each* line show the real uncertainties in these quantities.

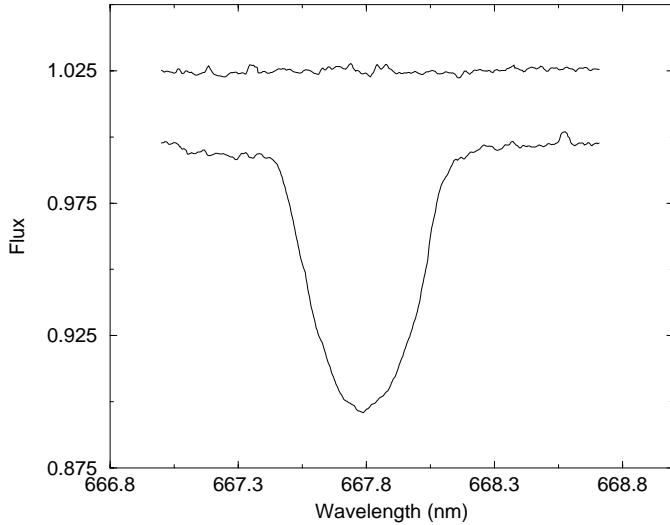


**Fig. 4.** The normalized He I 667.8 nm line profile for AR Cas reconstructed by KOREL. The null result for the secondary has been shifted upward for clarity

Systemic radial velocities for the various lines were determined by measuring the positions of the centres of the line profiles recovered by KOREL. In the case of the Si II 637.1 line, the secondary spectrum is most probably due to a different element, hence the more negative  $\gamma$  for this line.

The radial velocity curve for H $\alpha$  is shown in Fig. 5.

The peculiar shape of the secondary's H $\alpha$  profile is most likely due to small, unavoidable continuum rectification errors in this spectral region. Also, errors in the elements can affect the shape of a reconstructed profile by effectively combining adjacent radial velocity bins. In the present case, even small unavoidable errors in the elements can influence the shape of the secondary's line profile, and for very broad lines such as H $\alpha$  this effect is particularly noticeable. However, what is important is that the secondary has been detected at all. It is clear from the reconstructed profiles for He I 667.8 nm that the same “wave” effect is not present in this line and thus does not affect our ability to detect LPV (in fact, KOREL would ignore the LPV as just high frequency noise).

At this point, the skeptical reader may well be wondering about the reality of the secondary spectrum recovered by KOREL. As this component's spectrum is most sensitive to the mass ratio determined by KOREL, we let the program calculate another solution of the H $\alpha$  line, starting at a value of the mass ratio slightly different from the original value used. All other parameters were left unchanged. Moreover, KOREL was allowed initially to use a relatively large search interval (0.01) for the mass ratio. KOREL did indeed return to a value of the mass ratio very close to that found in the original solution, and hence we are fairly certain that the program did not find a local minimum in the parameter space of the orbital elements. It should also be appreciated that this is quite a stringent test, since the initial solution for H $\alpha$  was rather difficult on account of the presence of the telluric lines.

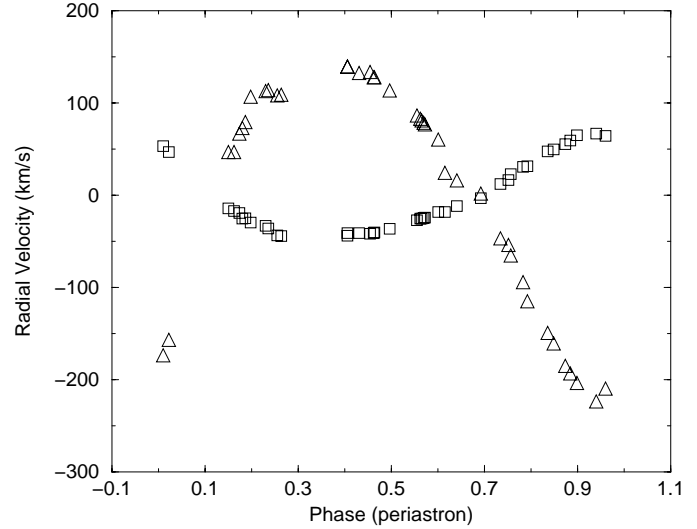


**Fig. 5.** The H $\alpha$  radial velocity curve for both components of AR Cas as determined by KOREL. The squares and triangles denote primary and secondary star data respectively

#### 4.3. Spectroscopic orbit of the primary based on all RVs

In addition to the KOREL results, a new orbital solution for the primary of AR Cas has been computed, based on both new (cross-correlation, i.e. zero-point calibrated) and published data (cf. Table 2). In total, there are 245 primary's RVs available. A series of solutions was computed, each incorporating different assumptions. These solutions are denoted as A, B, C, D, and E. Solution A: all parameters were solved for except the sidereal period  $P$ . Solution B:  $P$ ,  $T_{peri}$ , and  $e$  were fixed. Solution C:  $P$  and  $e$  were fixed. Solution D: Uniform weighting with  $P$ ,  $T_{peri}$ , and  $e$  fixed. Solution E: Uniform weighting with only one systemic velocity and  $P$ ,  $T_{peri}$ , and  $e$  fixed. These solutions were computed using FOTEL (Hadrava, 1990), allowing each data set to have its own systemic velocity (solutions A–D) and relative weight (solutions A–C, with the understanding that our new observations for which the RV zero points were calibrated through the use of the set of telluric lines were treated as originating from the same instrument). The weights were assigned according to the inverse squares of the rms residuals for each data set, computed during a prior run of FOTEL on the combined data set. They are also given in Table 2. Note that the numbering of the systemic velocities corresponds directly to the dataset number of Table 2. The orbital period and the rate of apsidal motion were kept fixed at values derived from photometry. For those solutions in which  $T_{peri}$  was fixed, we have used the value from the light curve solution, as it lies within the range of times covered by the published radial velocity data. Note the good agreement of the epoch of periastron with that derived from photometry. The orbital solutions are given in Table 9, and the corresponding phase diagram is shown in Fig. 6.

The various systemic velocities show differences which are formally significant, and this deserves some comment. Given that different workers used different instruments operating at various resolutions, and that in most cases they measured dif-

**Table 8.** AR Cas KOREL solutions.

Parameter	H $\alpha$	He I 667.8 nm	Ne I 640.2 nm	Si II 634.7 nm	Si II 637.1 nm
$\gamma_{pri}$ (km s $^{-1}$ )	$-14.5 \pm 0.6$	$-10.6 \pm 1.4$	$-15.5 \pm 3.4$	$-15.2 \pm 1.5$	$-9.67 \pm 1.7$
$\gamma_{sec}$ (km s $^{-1}$ )	$-12.0 \pm 2.2$			$-15.2 \pm 1.7$	$-29.4 \pm 2.0$
$T_{peri}$	$50278.662 \pm 0.036$	$50278.667 \pm 0.103$	$50278.647 \pm 0.216$	$50278.708 \pm 0.101$	$50278.694 \pm 0.121$
$e$	$0.242 \pm 0.009$	$0.243 \pm 0.023$	$0.259 \pm 0.051$	$0.255 \pm 0.021$	$0.243 \pm 0.025$
$\omega$ (deg)	$35.0 \pm 2.2$	$35.3 \pm 6.1$	$35.3 \pm 12.7$	$35.1 \pm 5.9$	$35.6 \pm 7.1$
$K_{pri}$ (km s $^{-1}$ )	$56.8 \pm 0.5$	$56.4 \pm 1.4$	$56.3 \pm 3.1$	$56.7 \pm 1.4$	$58.5 \pm 1.6$
$q$ (sec/pri)	$0.315 \pm 0.014$			$0.3046 \pm 0.0080$	$0.2757 \pm 0.0079$
Period (days)	6.0663170	6.0663170	6.0663170	6.0663170	6.0663170
$\pm\sigma_1$ (pri) (km s $^{-1}$ )	1.93	6.03	10.7	4.80	5.60
$\pm\sigma_1$ (sec) (km s $^{-1}$ )	8.13			5.50	6.50
$m_1 \sin^3 i$ ( $M_{\odot}$ )	$5.83 \pm 0.20$			$6.25 \pm 0.32$	$8.94 \pm 0.51$
$m_2 \sin^3 i$ ( $M_{\odot}$ )	$1.84 \pm 0.06$			$1.90 \pm 0.10$	$2.46 \pm 0.14$
$a_1 \sin i$ ( $R_{\odot}$ )	$6.60 \pm 0.06$			$6.57 \pm 0.17$	$6.80 \pm 0.19$
$a_2 \sin i$ ( $R_{\odot}$ )	$20.96 \pm 0.93$			$21.56 \pm 0.22$	$24.66 \pm 0.27$

ferent lines, one should not assign any physical interpretation to the differences in the systemic velocities. Indeed, a plot of these data as a function of epoch does not reveal any clear trend indicative of the influence of a third body, for example. The large negative value for  $\gamma_{10}$  is due to the fact that there are relatively few echelle data, and because of the low signal-to-noise ratio for the He I 667.8 nm line in this dataset. It is clear from Table 9 that the various assumptions make little difference in the solutions, so we have therefore adopted solution B. This solution also shows good agreement with the KOREL results.

#### 4.4. Independent estimates of the mass ratio

To carry out further checks on the mass ratio derived directly by KOREL, we did the following independent estimates:

##### 4.4.1. Mass ratio from the mass function and spectral type

It is possible to use the orbital solution based on the primary RVs only to obtain an estimate of the mass ratio which is independent of the results from KOREL. Adopting the orbital inclination of  $85^{\circ} 34$  from the light-curve solution and the mass function which follows from the orbital solution for the primary only, one gets  $q = 0.325$ , hence  $m_2 = 1.66 M_{\odot}$ . A primary mass of  $5.1 M_{\odot}$  was assumed, based on this star's spectral type and the tables of Harmanec (1988).

##### 4.4.2. Mass ratio from the Hipparcos parallax

Another way to obtain an independent estimate of the mass ratio is to adopt the Hipparcos parallax of AR Cas (Perryman et al. 1997). Ideally, one should also proceed using estimates of the stellar parameters independent of the photometric and spectroscopic orbits presented here.

The Hipparcos parallax for AR Cas is  $5.67 \pm 0.56$  mas, which translates to the distance modulus of  $6^m.23 \pm 0^m.21$ . The magnitude difference between the components is well-defined from the light curve and also from the H $\alpha$  line profiles reconstructed

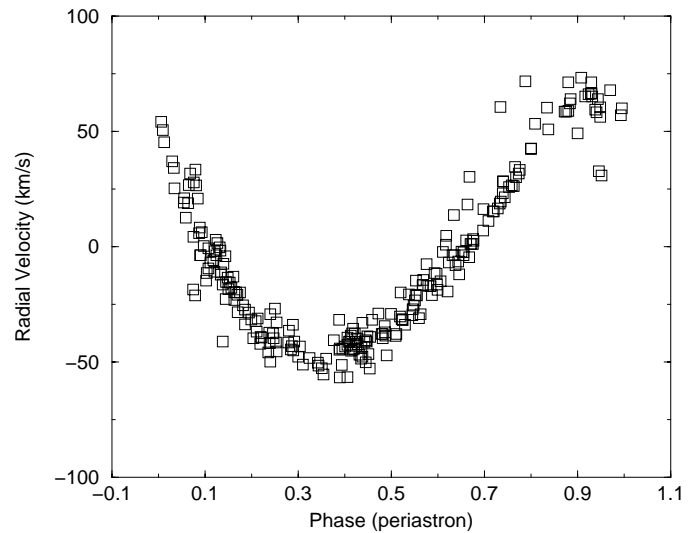


**Fig. 6.** The radial-velocity curve of the primary component of AR Cas based on all available data. The phase shift due to apsidal motion is apparent here

by KOREL. Both of these show that the primary effectively dominates the combined light at the wavelengths for which data are available. Therefore, the observed colours can be taken as representative for the radiative properties of the primary. The photometric colors of AR Cas may be used to estimate the effective temperature and logarithmic surface gravity of the primary component. For this purpose, the Strömgren colors collected in the SIMBAD listing for AR Cas, and the calibrations of Napiewotzki et al. (1993) are the most suitable. Table 10 summarizes these results.

The calibration of Napiewotzki et al. gives an effective temperature of 17200 K and  $\log g = 4.10$  which translates to a spectral type of B4V for the primary of AR Cas. (Note that this is consistent with the most frequent spectral classification of B3V). Adopting these values, we have  $\log T_{\text{eff}} = 4.235$  and  $BC = -1.69$  from Popper's (1980) calibration. Estimating the

**Table 9.** AR Cas single-lined orbits.  $\dot{\omega} = 5.80 \times 10^{-4} \text{ deg day}^{-1}$  has been assumed

Parameter	Solution				
	A	B	C	D	E
Period (d)	6.0663170	6.0663170	6.0663170	6.0663170	6.0663170
$T_{\text{peri}}$	$36847.807 \pm 0.039$	36847.9381	$36847.811 \pm 0.034$	36847.9381	36847.9381
$e$	$0.219 \pm 0.008$	0.240	0.240	0.240	0.240
$\omega$ (deg)	$32.9 \pm 2.3$	$40.5 \pm 5.0$	$32.8 \pm 2.1$	$42.8 \pm 0.8$	$42.0 \pm 0.9$
$K$ (km s $^{-1}$ )	$55.5 \pm 0.5$	$55.6 \pm 0.5$	$55.9 \pm 0.5$	$55.8 \pm 1.0$	$54.7 \pm 1.0$
$\gamma_1$ (km s $^{-1}$ )	$-17.8 \pm 5.3$	$-18.2 \pm 5.5$	$-17.8 \pm 5.5$	$-18.6 \pm 5.1$	$-13.1 \pm 0.6$
$\gamma_2$ (km s $^{-1}$ )	$-17.4 \pm 1.5$	$-17.3 \pm 1.6$	$-17.2 \pm 1.5$	$-17.2 \pm 1.3$	
$\gamma_3$ (km s $^{-1}$ )	$-10.0 \pm 1.0$	$-10.2 \pm 1.0$	$-10.0 \pm 1.1$	$-10.0 \pm 1.1$	
$\gamma_4$ (km s $^{-1}$ )	$-12.9 \pm 0.6$	$-12.9 \pm 0.6$	$-12.9 \pm 0.6$	$-13.1 \pm 0.7$	
$\gamma_5$ (km s $^{-1}$ )	$-11.7 \pm 1.1$	$-11.8 \pm 1.1$	$-11.4 \pm 1.1$	$-11.8 \pm 1.2$	
$\gamma_6$ (km s $^{-1}$ )	$-8.7 \pm 0.9$	$-8.9 \pm 0.9$	$-8.7 \pm 0.9$	$-8.33 \pm 1.0$	
$\gamma_7$ (km s $^{-1}$ )	$-14.3 \pm 1.3$	$-15.0 \pm 1.1$	$-14.6 \pm 1.1$	$-15.0 \pm 1.3$	
$\gamma_8$ (km s $^{-1}$ )	$-14.2 \pm 1.0$	$-14.5 \pm 1.0$	$-14.2 \pm 1.0$	$-15.2 \pm 1.1$	
$\gamma_9$ (km s $^{-1}$ )	$-11.3 \pm 0.7$	$-11.3 \pm 0.8$	$-11.3 \pm 0.8$	$-10.5 \pm 1.1$	
$\gamma_{10}$ (km s $^{-1}$ )	$-32.6 \pm 4.2$	$-32.5 \pm 3.9$	$-32.7 \pm 4.3$	$-32.2 \pm 4.2$	
$f(M)$ ( $M_{\odot}$ )	$0.100 \pm 0.003$	$0.099 \pm 0.003$	$0.101 \pm 0.003$	$0.100 \pm 0.005$	$0.094 \pm 0.005$
$a \sin i$ ( $R_{\odot}$ )	$6.49 \pm 0.06$	$6.47 \pm 0.06$	$6.50 \pm 0.06$	$6.49 \pm 0.12$	$6.36 \pm 0.12$
$\pm \sigma_1$ (km s $^{-1}$ )	8.52	8.76	8.70	8.62	9.70

**Table 10.** *uvby* photometric colors of AR Cas

Parameter	Observed	Intrinsic
$V$	4 <sup>m</sup> 91	4 <sup>m</sup> 73
$b - y$	-0 <sup>m</sup> 045	-0 <sup>m</sup> 084
$u - b$	0 <sup>m</sup> 389	0 <sup>m</sup> 330
$[u - b]$	-	0 <sup>m</sup> 458
$m_1$	0 <sup>m</sup> 086	0 <sup>m</sup> 099
$c_1$	0 <sup>m</sup> 307	0 <sup>m</sup> 300
$\beta$	2 <sup>m</sup> 681	-
$E(b - y)$	-	0 <sup>m</sup> 039
$E(B - V)$	-	0 <sup>m</sup> 054

mass of the primary to be  $5.1 M_{\odot}$ , we can use the parallax, the primary radius from the light curve solution, and Kepler's third law to derive a mass ratio of  $q = 0.383$ . When one takes into account the errors in all of the quantities contributing to  $q$ , the resulting error is greater than  $q$  itself:  $q = 0.383 \pm 0.450$ . Nevertheless, one can conclude that the mass ratio of AR Cas implied by its observed parallax and radiative properties is consistent with that derived from the spectroscopic orbit. The contributions of the different parameters to the error in the mass ratio are summarised in Table 11 (these are the different terms which, when added in quadrature, give the error in the mass ratio). Thus, the error in the mass ratio is dominated by the errors in the parallax and effective temperature.

## 5. Basic physical parameters

### 5.1. Masses and radii

The masses of the components of AR Cas may be determined from the KOREL orbital solutions. For this purpose, we have

**Table 11.** Error contributions to the estimated mass ratio.

Parameter	value	error
$V$ (mag)	4.739	0.02
$T_{\text{eff}}$ (K)	17200	0.2
$r_{\text{pri}}$	0.1826	0.04
$\pi$ (arcsec)	0.00567	0.4
$M$ ( $M_{\odot}$ )	5.1	0.03

adopted the orbit based on  $H\alpha$ , as the secondary parameters were deemed to be determined better than for the other lines. However, similar results are obtained with the Si II 634.7 nm line. The inclination is well-determined from the light curve, and the resulting masses are given in Table 12. To determine the errors in  $T_{\text{eff}}$  for both components, we have varied each component's mass and radius by their respective errors, and then used the tables of Harmanec (1988) to see what range in  $T_{\text{eff}}$  such errors correspond to. In the case of the primary star, this error is probably underestimated since we do not know the precision of the photometric colors used to derive its temperature.

The effective temperature of the secondary in Table 12 is based on the spectral type of A5V implied by its mass, once again using the calibration data of Harmanec (1988). However, this star's radius indicates a spectral type of A9-F0 from the same calibration. A spectral type of A7-8V is implied by  $M_{\text{bol}}$  for the secondary using the same calibration. On this basis, and considering the uncertainties in the mass, radius, and  $M_{\text{bol}}$ , we adopt a spectral type of A6-7V for this star. It should be mentioned here that the discrepancy between mass, radius and temperature is due to the weak dependence of these parameters on spectral type combined with observational errors. We also ten-

**Table 12.** Basic physical quantities of AR Cas

Parameter	Primary	Secondary
$M (M_{\odot})$	$5.90 \pm 0.20$	$1.86 \pm 0.06$
$R (R_{\odot})$	$5.05 \pm 0.06$	$1.60 \pm 0.03$
$T_{\text{eff}} (K)$	$17200 \pm 500$	$8150 \pm 200$
$\log g$ (cgs)	$3.80 \pm 0.02$	$4.30 \pm 0.02$
$M_{\text{bol}}$ (mag)	$-3.56 \pm 0.13$	$2.18 \pm 0.11$
BC (mag)	-1.69	-0.020
$M_V$ (mag)	$-1.87 \pm 0.13$	$2.20 \pm 0.11$

tatively suggest that the secondary may be an Am star, as these objects display this kind of behaviour (Conti 1970).

The stellar radii follow from the total semi-major axis from the KOREL orbit and the relative radii from the final light-curve solution. They are also given in Table 12.

### 5.2. Projected rotational velocities

Different values of  $v \sin i$  for the primary star have been presented in the literature. Gaida and Seggewiss (1981) give  $v \sin i = 120 \pm 30 \text{ km s}^{-1}$ . We have used the SYNSPEC program of Hubeny et al. (1994) to generate model atmosphere fluxes to compare with the line profiles recovered by KOREL. We have used the Kurucz (1993b) grid of solar composition LTE line blanketed models and the line list of Kurucz (1993a) as input for SYNSPEC. A plane parallel geometry has been assumed in these calculations, as have hydrostatic and radiative equilibria. An LTE model atmosphere spectrum corresponding to the parameters of the primary star ( $T_{\text{eff}} = 17000 \text{ K}$ ,  $\log g = 4.0$ ) was convolved with a rotational line profile having  $v \sin i = 120 \text{ km s}^{-1}$ . This theoretical spectrum agrees very well with the primary  $H\alpha$  line profile recovered by KOREL, and in particular the C II lines in the red wing of  $H\alpha$  are fitted quite well (Fig. 7). The light ratio from the light curve solution was used to correct the component  $H\alpha$  line profile for the magnitude difference between the components. However, the agreement is not as good for the other metal line profiles and He I 667.8 nm. A large non-LTE effect is expected for the latter, but the observed disagreement by about a factor of 2 in terms of line depth with the primary's Si II 634.7–7.1 nm and Ne I 640.2 nm lines is unexpected. The projected rotational velocity  $v \sin i$  of the primary was also computed independently using the three He I 667.8 nm line profiles obtained at  $0.48 \text{ nm mm}^{-1}$ . For this purpose the Fourier–Bessel transform method (Deeming, 1977, and Pitters et al. 1996) was used. A mean  $v \sin i = 129.3 \text{ km s}^{-1}$  was found, in good agreement with the value presented by Gaida and Seggewiss. From its radius, the orbital period, and the inclination, a synchronous rotational velocity for the primary star of  $43 \text{ km s}^{-1}$  was determined, which is exactly one-third of the measured  $v \sin i$ . Following Pan (1997), the synchronous rotational velocity at periastron is then  $70 \text{ km s}^{-1}$ , which is a factor of about 1.8 lower than the measured  $v \sin i$ .

From the new light curve solution, we can show that the synchronous projected rotational velocity of the secondary is

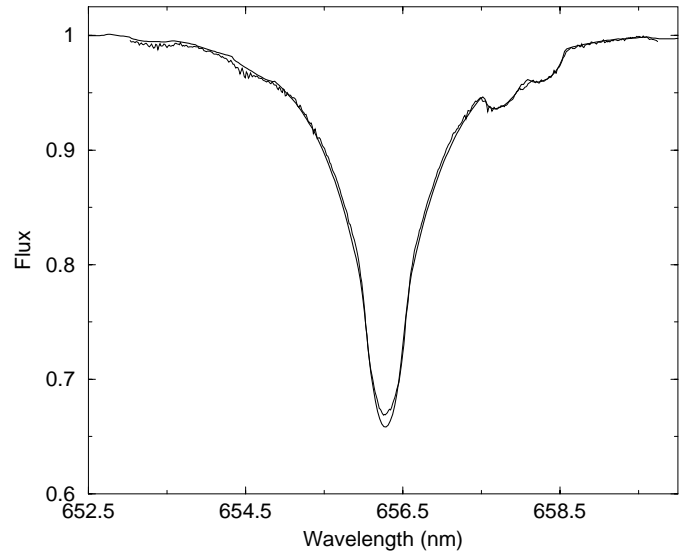


**Fig. 7.** Comparison of an LTE model (heavy line) with the primary star normalized  $H\alpha$  line profile (see text, Sect. 5.2)

$13 \text{ km s}^{-1}$ . This star's mass indicates a spectral type of about A6V, so that its effective temperature must be close to 7950 K, assuming that  $\log g = 4.0$ . A synthetic spectrum corresponding to these values of effective temperature and surface gravity was generated and compared with the secondary's Mg II 448.1 nm line profile recovered by KOREL and adjusted for the light ratio at this wavelength. This comparison is shown in Fig. 8, and there is remarkably good agreement between the observed and synthetic spectra. This agreement can be taken to show that our results for AR Cas, both photometric and spectroscopic, provide a self-consistent model for this star.

### 5.3. Apsidal motion

The observed apsidal motion rate determined from the light curve solution may be used, along with the physical parameters, to compute the internal structure constant (ISC)  $\log \bar{k}_2$  for AR Cas. This allows a comparison between the observed ISC and that predicted by stellar structure theory (Claret and Giménez 1993). In the following discussion, we have incorporated both tidal and rotational distortion terms in calculating  $\log \bar{k}_2$ . In general, the observed value of  $\log \bar{k}_2$  is a weighted mean value for both components. However, in the case of AR Cas, the primary star's mass and radius are such that it provides the dominant contribution to  $\log \bar{k}_2$ . On the basis of the physical parameters just presented, we find an observed value of  $\log \bar{k}_2 = -2.622 \pm 0.060$ . The corresponding theoretical value is  $-2.380$  as it follows from Table 16 of Claret and Giménez (1992). The errors in the physical parameters do allow the latter value to change by about  $\pm 0.1$ . At first glance, there would appear to be some contradiction between observation and theory, but given that the apsidal period is  $U = 1938 \pm 207 \text{ yr}$ , it is clear that the current observations have not covered a large fraction, only about 4 percent, of the apsidal period. Therefore, one can say that the observed and theoretical  $\log \bar{k}_2$  values are

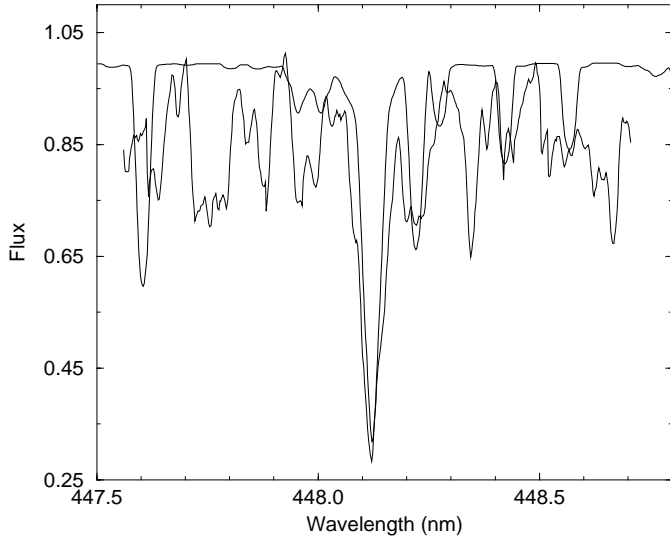


**Fig. 8.** Comparison of an LTE model (heavy line) with the secondary star Mg II 4481 nm line profile

in agreement, but that further observations, particularly times of eclipse minima, are required to confirm this agreement.

## 6. Line profile variability

Examination of the Reticon, CCD, and echelle data show that line profile variability (LPV) is present in AR Cas, and is particularly obvious in the He I 667.8 nm and He I 492.0 nm lines. It should be mentioned here that both DH and SY identified the LPV in AR Cas on different occasions, and independently of one another. To explore the LPV, we have computed a KOREL solution for He I 667.8 nm and generated a set of difference spectra (in the rest frame of the primary star) using the primary star's line profile as recovered by KOREL. We make use of these difference spectra in the following discussion.

A temporal variance spectrum (TVS, Fullerton et al. 1996) formed from all available CCD He I 667.8 nm line profiles, with all data being weighted according to signal-to-noise, shows that LPV is present in this line (Fig. 9). The orbital radial velocity shifts have been accounted for in forming this TVS. We also show a TVS for a particular subset (dotted line in Fig. 9) obtained by SY on a single night. Note that because data from different detectors were used, that it was not possible to perform the same statistical test on this TVS as described by Fullerton et al. Moreover, it is not clear how a given CCD spectrum should be weighted, since each one-dimensional spectrum is generated by averaging several rows of a two-dimensional frame. A TVS for He I 492.0 nm also demonstrates that LPV is present.

The best documentation for LPV comes from the He I 667.8 nm line profiles obtained at  $0.48 \text{ nm mm}^{-1}$ , as the changes in shape during and between successive nights are quite clear. In Fig. 10 we present difference spectra generated from data taken on a single night. An absorption “dip” at about 667.9 nm appears to move redward during this time sequence of spectra. The difference spectra in this figure were generated using the primary

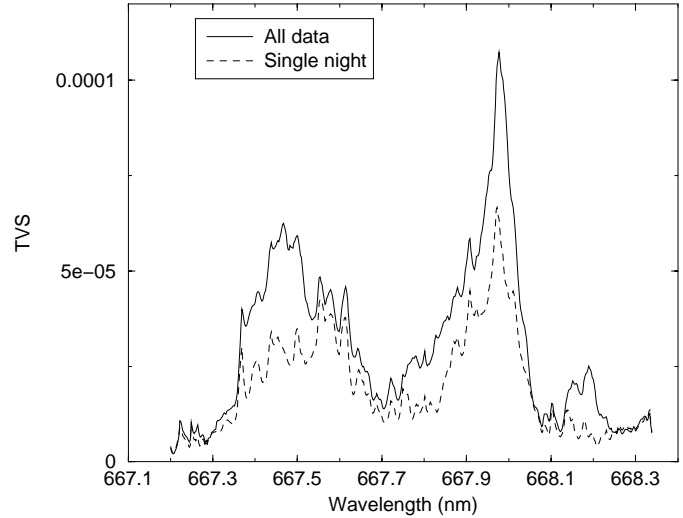


**Fig. 9.** Temporal variance spectrum for the He I 667.8 nm line profile data (see text for details)

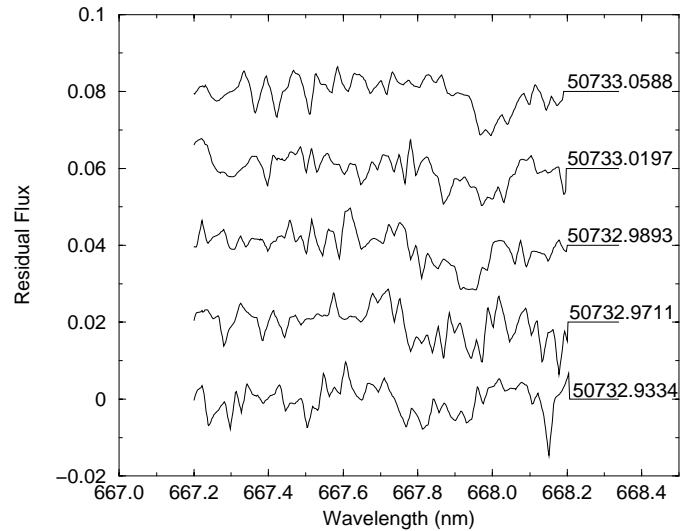


**Fig. 10.** He I 667.8 nm difference spectra generated from line profile data obtained at  $0.48 \text{ nm mm}^{-1}$ . Each difference spectrum is labelled according to its heliocentric Julian date. The wavelength scale is that of the primary star. The residual flux scale is arbitrary and each difference spectrum has been shifted upward by a constant amount for clarity

star's line profile recovered by KOREL, and the wavelength scale is that of the primary star, i.e., the primary's systemic radial velocity has *not* been subtracted. Also, the He I 492.0 nm profiles from the echelle data show the LPV quite well, with difference spectra from a KOREL decomposition of this line showing clear night-to-night changes (Fig. 11).

The difference spectra generated by KOREL were used as input for a Fourier-Doppler imaging (FDI) program (Telting and Schrijvers, 1997). Essentially, for each radial velocity bin across the line, a Lomb-Scargle periodogram was computed, for the frequency range  $0-5 \text{ c d}^{-1}$ . No clear periodicity was revealed by this calculation, but it is apparent that most of the spectral power lies in the interval from  $1.5 \text{ c d}^{-1}$  to  $2.5 \text{ c d}^{-1}$ . However,

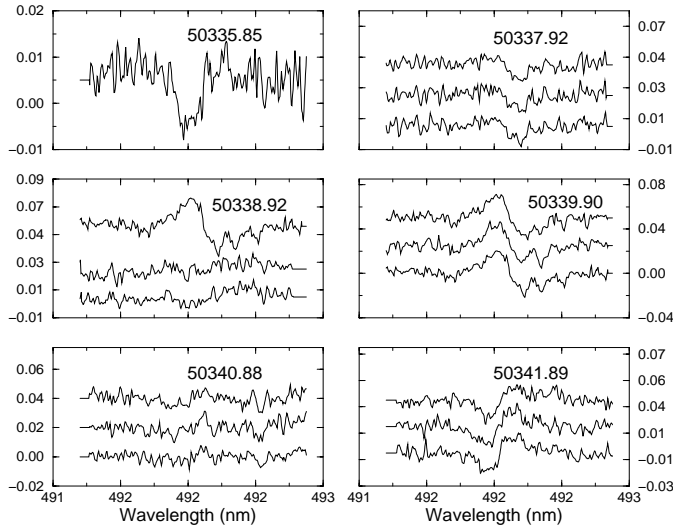


**Fig. 11.** He I 492.0 nm difference spectra, obtained with the San Pedro Mártir echelle spectrograph. The spectra are organized according to HJD. In each panel, the vertical scale corresponds to residual flux, with the difference spectra being shifted vertically for clarity. Each panel has the same wavelength scale, which is that of the primary star, i.e., no correction for the systemic radial velocity has been applied. The “bumps” indicate the presence of LPV in this line.

we should caution that with the FDI method it is perhaps better to have a longer *continuous* data set than that which we have at present.

Further support for the presence of LPV in AR Cas comes from examining the mode radial velocity of He I 667.8 nm. The mode radial velocity is defined (L.A. Balona, priv. comm.) as the velocity corresponding to the line minimum. This was measured on each spectrum by fitting a parabola to the 10 points bracketing the line minimum. After removing the orbital radial velocity variation, the residuals were subject to a Lomb–Scargle periodogram analysis. A frequency range of  $0 \text{ c d}^{-1}$  up to  $12 \text{ c d}^{-1}$  was scanned. The maximum spectral power was found at a frequency of  $1.96 \text{ c d}^{-1}$ , with a false alarm probability of  $6.72 \times 10^{-3}$ , indicating a highly significant peak (Horne and Baliunas, 1986). The number of independent frequencies  $N_i = 68.8$  (see Horne and Baliunas for a definition of  $N_i$ ). These results should be interpreted with some caution because of the presence of 1-d aliases in the power spectrum.

All of the results above suggest that LPV is indeed present in AR Cas, and that any periodic signal corresponding to the LPV has a period of less than one day. However, to refine the LPV period will require a longer *continuous* time series of line profile data, preferably obtained over several consecutive nights.

## 7. Summary

New spectroscopic and photometric data are presented which, together with published data, have allowed us to derive new physical parameters for AR Cas. Application of the KOREL spectral disentangling program has allowed us to recover the spectrum of the secondary star, and to identify its spectral type

as A6V. For the primary and secondary, respectively, we find:  $m_1 = (5.90 \pm 0.20) M_{\odot}$ ,  $m_2 = (1.86 \pm 0.06) M_{\odot}$ ,  $r_1 = (5.05 \pm 0.06) R_{\odot}$ ,  $r_2 = (1.60 \pm 0.03) R_{\odot}$ ,  $T_1 = 17200 \pm 500 \text{ K}$ , and  $T_2 = 8150 \pm 200 \text{ K}$ . We suggest as well that the secondary may be an Am-type star. Furthermore, we have demonstrated the existence of apsidal motion. Analyses of a set of He I 667.8 nm line profiles has shown that line profile variability is present, but we are unable to identify a period for this effect.

**Acknowledgements.** The authors would like to thank an anonymous referee for comments on an earlier version of this paper. We would like to thank our colleagues P. Koubský, and J. Kubát for obtaining some of the spectra used in this study. DH would like to thank Dr. G. Scholz of the Astrophysikalische Institut Potsdam for obtaining the paper by Luyten et al., which was not available at Ondřejov, and Dr. K. Olah of Konkoly Observatory, Budapest, for obtaining the paper by Gorza and Heard. DH and SY would like to thank the director and staff of the Dominion Astrophysical Observatory respectively for generous allocation of observing time and technical assistance. This work is partially based on observations obtained at the San Pedro Mártir observatory, a facility operated by UNAM, México. P. Harmanec and P. Eenens acknowledge allocation of observing time there. The use of the computerized bibliography from the Strasbourg Astronomical Data Centre is gratefully acknowledged. This study was supported by the grant 205/96/0162 of the Grant Agency of the Czech Republic, by grant A3003805 of the Grant Agency of the Academy of Sciences, and by the project K1-003-601/4 *Astrophysics of non-stationary stars* of the Academy of Sciences of the Czech Republic, and partly by the Research Council of Turkey.

## Appendix A: details of the reduction and transformation of photometric data

The 1997 *uvby* observations were secured by Hasan Ak with the 0.40-m reflector of the Turkish National Observatory, Turkey, equipped with a SSP5A photometer. The 1998 *UBV* observations were secured by Hrvoje Božić at Hvar, Croatia with a 0.65-m reflector and an EMI6265S tube, and by Petr Harmanec with the 0.84-m reflector of San Pedro Mártir Observatory, Mexico. 1 Cas and  $\sigma$  Cas served as the comparison and check star, respectively. The check star was observed as frequently as the variable. In all cases, constant stars, for which accurate all-sky *UBV* magnitudes were derived by Harmanec, Horn & Juza (1994) were also observed and used to the determination of nightly (linear extinction and zero-point drifts) and seasonal (including colour extinction) transformations to the standard system. All these reductions were carried out by P. Harmanec with the help of the reduction package HEC22/VYPAR (see Harmanec et al. 1994 and Harmanec & Horn 1998 for the detailed description and the programs and all necessary data files). As a by-product of these reductions, we also derived the improved *UBV* magnitudes of the comparison star 1 Cas which were then used with all datasets. All these observations will be later deposited at the Strasbourg Astronomical Data Centre. We deliberately postpone their release since our observations will continue and we shall still slightly improve the data reduction after the season is completed. However, we encourage interested colleagues to ask for the data via e-mail (PH at [hec@sunstel.asu.cas.cz](mailto:hec@sunstel.asu.cas.cz)) in advance of publication.

**Table A1.** A detailed list of particular magnitude differences used to define the transformation of the Lick  $m_{500}$  magnitudes to the  $V$  magnitude of the Johnson system. Note that Stebbins measured integrated light of both components of  $\zeta$  Lyr. Correspondingly, we also calculated their integrated  $UBV$  magnitudes and colours. Whenever available, the accurate  $UBV$  values derived either by Harmanec et al. (1994) or by us here were adopted. In all other cases, Johnson et al. (1966) mean values were used to calculate the respective differences. The  $O - C$  deviations of the bilinear fit are also given

Objects used	$dV - dm$	$d(B - V)$	$d(U - B)$	$dm$	$dV$	$O - C$
$\eta$ Lyr – $\gamma$ Lyr	0.030	–0.069	–0.608	1.124	1.154	0.025
$\gamma$ Lyr – $\delta$ Her	0.064	–0.151	–0.132	0.054	0.118	0.036
$\gamma$ Lyr – $\zeta$ Her	0.467	–0.721	–0.262	–0.015	0.452	0.005
$\eta$ Lyr – $\zeta_{1+2}$ Lyr	0.269	–0.349	–0.799	0.054	0.323	–0.030
$\lambda$ Aql – $\theta$ Aql	0.005	–0.020	–0.150	0.178	0.183	0.010
1 Cas – $\sigma$ Cas	–0.045	0.041	–0.055	–0.010	–0.055	0.019
by definition	0.000	0.000	0.000	0.000	0.000	0.000

We also attempted to transform some of the published data sets into the standard  $UBV$  system. For the Hipparcos  $H_p$  magnitudes (dataset 5 of Table 3), this problem was solved by Harmanec (1998) and we simply used the transformation formula derived by him and  $B - V$  and  $U - B$  derived by us to obtain the standard Johnson  $V$  magnitudes of AR Cas and also 1 Cas and  $\sigma$  Cas.

We attempted to derive also a transformation of Stebbins (1921) observations into the standard Johnson  $V$  magnitude. These Lick observations were secured with a diode having maximum sensitivity near 500 nm, i.e. somewhere between the  $B$  and  $V$  bands but closer to  $V$ . Fortunately, Stebbins published the observed magnitude difference between  $\sigma$  Cas and 1 Cas. In his study of  $\beta$  Lyr, Stebbins (1916) also published observed magnitude differences between several other constant stars.

Since the standard  $(B - V)$  and  $(U - B)$  values for all these stars are known, it is possible to define a transformation between the Johnson  $V$  and the old Lick  $m_{500}$  magnitude in the form

$$V - m_{500} = a(B - V) + b(U - B) + c,$$

where  $a$ ,  $b$  and  $c$  are the transformation coefficients. In practice, however, one has to use this transformation in a differential form since only magnitude differences between various two stars are available for the Lick data, i.e.

$$dV - dm_{500} = a d(B - V) + b d(U - B),$$

where  $dV$  etc. denote the respective magnitude and colour differences between two stars. Our least-squares fit to the data which are detailed in Table A1 resulted in the following transformation formula

$$dV = dm_{500} - 0.64915 d(B - V) - 0.01603 d(U - B).$$

The rms error of the fit per one observation is  $0^m.021$  only, a remarkable result considering circumstances. We used the following standard colour differences AR Cas – 1 Cas:

$$d(B - V) = -0^m.083 \quad \text{and} \quad d(U - B) = 0^m.201.$$

We found no possibility how to transform also CR71 and GK73 data into the standard system. We, therefore, only added our

improved magnitudes of 1 Cas to the respective magnitude differences AR Cas – 1 Cas and otherwise left these observations on their instrumental systems. However – since blue and yellow filters were used in both cases and since the transformation terms in  $(B - V)$  are always found smaller than about 0.3 in such circumstances, we do believe that even these data sets are on the system of Johnson's  $V$  and  $B$  magnitudes within less than  $0^m.02$  ( $= -0^m.083 \times 0.3$ ).

## References

- Baker R.H., 1910, Publ. Allegheny Obs. 2, 28  
Catalano S., Rodonò M., 1971, AJ 76, 557.  
Claret A., Giménez A., 1992, A&AS 96, 255  
Claret A., Giménez A., 1993, A&A 277, 487  
Conti P.S., 1970, PASP 82, 781  
Deeming T.J., 1977, Ap&SS 46, 13  
Fullerton A.W., Gies D.R., Bolton C.T., 1996, ApJ 103, 475  
Gaida M., Seggewiss W., 1981, Acta Astron. 31, 231  
Gordon K.G., Kron G.E., 1973, Ap&SS 23, 403  
Gorza W.L., Heard J.F., 1971, Publ. David Dunlap Obs. 3, 99  
Hadrava P., 1990, Contr. Astron. Obs. Skalnaté Pleso 20, 23  
Hadrava P., 1997, A&AS 122, 581  
Harmanec P., 1988, Bull. Astron. Inst. Czechosl. 39, 329  
Harmanec P., 1998, A&A 335, 173  
Harmanec P., Horn J., 1998, Journal Astron. Data No. 4 CD-ROM file 5  
Harmanec P., Horn J., Juza K., 1994, A&AS 104, 121  
Harmanec P., Hadrava P., Yang S., et al., 1997, A&A 319, 867  
Holmgren D., 1996, In: Chochol D., Skopal A., Pribulla T. (eds.) Physical Processes in Interacting Binaries. Astronomical Institute of the Slovak Academy of Sciences, Tatranská Lomnica, p. 20  
Holmgren D., Hadrava P., Harmanec P., Koubský P., Kubát J., 1997, A&A 322, 565  
Horn J., Kubát J., Harmanec P., et al., 1996, A&A 309, 521  
Horne J.H., Baliunas S.L., 1986, ApJ 302, 757  
Hubeny I., Lanz T., Jeffery C.S., 1994, In: Jeffery C.S. (ed.) Newsletter on Analysis of Astronomical Spectra No. 20, St. Andrews University, p. 30  
Huffer C.M., Collins G.W., 1962, ApJS 7, 351  
Johnson H.L., Mitchell, Iriarte B., Wisniewski W.Z., 1966, Comm. Lunar Planet Obs. 4, 99  
Kurucz R.L., 1993a, Atomic Data for Opacity Calculations. Kurucz CD-ROM No. 1

- Kurucz R.L., 1993b, Solar Abundance Model Atmospheres. Kurucz CD-ROM No. 19
- Luyten W.J., Struve O., Morgan W.W., 1939, Publ. Yerkes Obs. 7, 251
- Napiwotzki R., Schönberner D., Wenske V., 1993, A&A 268, 653
- Pan K., 1997, A&A 321, 202
- Perryman M.A.C, Høg E., Kovalevsky J., Lindegren L., Turon C., 1997, ESA SP-1200, The Hipparcos and Tycho Catalogues
- Petrie R.M., 1944, AJ 51, 22
- Piters A.J.M., Groot P.J., van Paradijs J., 1996, A&AS 118, 529.
- Popper D.M., 1980, ARA&A 18, 115
- Richardson E.H., 1968, J.R.Astron.Soc.Can. 62, 313
- Stebbins J., 1916, Lick Obs. Bull. 8, No. 277, 186 & 192
- Stebbins J., 1921, ApJ 54, 81
- Škoda P., 1996, In: Jacoby G.H., Barnes J. (eds.) Astronomical Data Analysis Software and Systems V, ASP Conference Series Vol. 101, ASP, San Fransisco, 187
- Telting J.H., Schrijvers C., 1997, A&A 317, 723